

Available online at www.sciencedirect.com

SCIENCE @ DIRECT®

Applied Surface Science xxx (2005) xxx–xxx

applied
surface sciencewww.elsevier.com/locate/apsusc

Surface plasmon resonance spectroscopy on rotated sub-micrometer polymer gratings generated by UV-laser based two-beam interference

M. Csete^{a,*}, G. Szekeres^a, Cs. Vass^a, N. Maghelli^b, K. Osvay^a,
Zs. Bor^a, M. Pietralla^b, O. Marti^b

^a Department of Optics and Quantum Electronics, University of Szeged, Dóm tér 9,
H-6720 Szeged, Hungary

^b Department of Experimental Physics, University of Ulm, Albert Einstein Allee 11, D-89069 Ulm, Germany

Received 3 May 2005; accepted 15 July 2005

Abstract

Two-beam interference method was applied to generate gratings having periods of 416 nm and 833 nm by the forth harmonic of a Nd:Yag laser on thin poly-carbonate films spin-coated onto silver layer-covered substrates. The dependence of the modulation depth on the fluence and number of laser pulses was investigated by atomic force microscopy. A secondary pattern appeared on very thin polymer layers thanks to the “p” polarized laser beam illumination induced self-organized processes. The conditions of the emergence of grating-coupling caused additional plasmon resonance peak were determined for the sub-micrometer periodic polymer gratings. Surface plasmon resonance measurements were performed in attenuated total reflection arrangement to determine the effect of the angle between the plasmon propagation direction and the polymer groves on the grating-coupling. The effect of the modulation depth on the grating-coupling caused additional resonance minimum was also analyzed. We found coupling phenomena according to our calculations, the differences between the measured and theoretically predicted resonance curves were explained by the scattering on the complex surface structure.

© 2005 Elsevier B.V. All rights reserved.

Keywords: Surface plasmons; Sub-micrometer polymer gratings; Grating-coupling

1. Introduction

The dependence of the field of plasmons excited in metals on the surface properties is widely investigated and applied phenomenon. The most preferred configuration to investigate the plasmons excited by light is the attenuated total reflection arrangement of Kretschmann [1]. The analyzes of the resonance characteristic of plasmons can be performed modifying the wave vector of the plasmons by changing the angle of incidence of a monochromatic light, or tuning the wavelength of the exciting light at the same angle of incidence. The constant wavelength method is appropriate to determine the optical thickness of a dielectric over-coating layer [2], and to qualify the surface roughness based on the broadening of the resonance curves [3,4].

The high sensitivity of the method allows to determine very small changes in the thickness, in this way the detection of small amount of material removed from or adhered on the surface is possible [5]. The presence of individual or periodic sub-wavelength metal objects on the surface causes interesting changes in the resonance characteristic of the plasmons, and the localization and grating-coupling effects are mainly studied at constant angle via wavelength tuning [6,7]. Ultrasensitive biosensors were developed based on silver nanoparticles, and wavelength-dependent localized surface plasmon resonance spectroscopy was applied to detect attached bio-molecules [8]. The grating-coupled surface plasmon resonance on metal-coated surfaces is also applied in biosensorization [9].

The purpose of our present study was to find the appropriate period, modulation depth, and rotation angle, where the grating-coupling phenomenon is detectable in presence of a sub-micrometer polymer grating. The applied experimental methods are detailed in Section 2. The sub-micrometer polymer

* Corresponding author.

E-mail address: mcsete@physx.u-szeged.hu (M. Csete).

gratings were generated by two-beam interference technique on special ATR substrates. We utilized the ATR method to excite plasmons by monochromatic light at the interface of thin silver layer and the over-coating, periodically structured polymer films. We performed combined atomic force microscopy and angle dependent SPR measurements to determine the sensitivity of the grating-coupling effect to the modulation depth.

The influence of the laser treatment conditions on the surface structure; the theoretical prediction of the dependence of the grating-coupling phenomenon on the properties and orientation of the polymer grating; the experimental proof of the grating-coupling in case of appropriate conditions and the explanation of the structure development are presented in Section 3. The conclusions of the present investigation concerning the applicability of “rotated grating-coupling” phenomenon to detect material adherence onto the surface are described in Section 4.

2. Experimental

2.1. Preparation of layered ATR substrates

NKB7 glass substrates (Geodasy) having a thickness of 2 mm were evaporated by double layer of 20 nm Al_2O_3 and 50 nm Ag. The presence of the aluminum-oxide does not cause broadening of the resonance curve measurable on pure silver, but promotes the silver adhesion. The metal surface was spin-coated by thin poly-carbonate films. PC grains (Bayer, MW: 24 000) were dissolved in chloroform and the spin coating was performed from solutions having 10 mg/ml concentration at 2500 rotation/min speed of spinning.

2.2. Grating generation by two-beam interference

We generated sub-micrometer periodic polymer gratings by master grating based two-beam interference method [10]. Two different master gratings (Spectrogon, PUV, 600 lines/mm and 1200 lines/mm) were illuminated by the fourth harmonic of a Nd:Yag laser ($\lambda_{\text{FH}} = 266 \text{ nm}$) in the experimental arrangement presented in Fig. 1a. The spatial filtering realized in both of the green and UV light-lines ensured clear Gaussian intensity distribution of the incoming beam. The diffraction efficiency was 30% for both of the first order-diffracted beams. The average fluence of the combined beams at the target plane was tuned in the region of $F_{\text{av}} = 8.32\text{--}15.6 \text{ mJ/cm}^2$ by rotating a half-wave plate after the frequency doubling.

The fluence and number of laser pulses were varied in order to modify the modulation depth of the resulted topographical structure.

2.3. Surface plasmon resonance spectroscopy on rotated sub-micrometer polymer gratings

Surface plasmons were excited in the attenuated total reflection (ATR) arrangement of Kretschmann. The geometry applied to study the plasmon resonance in presence of polymer gratings is presented in Fig. 1b. An NBK7 semi-cylinder

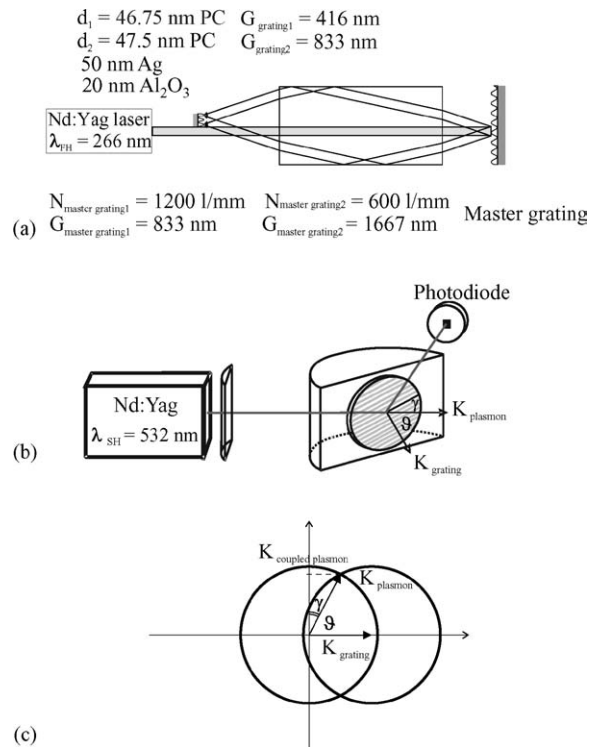


Fig. 1. (a) The experimental setup applied to generate grating via two-beam interference by the fourth harmonic of a Nd:YAG laser; (b) attenuated total reflection arrangement utilized to investigate the dependence of the reflected intensity on the angle of incidence in presence of rotated grating; (c) the condition of the grating coupling.

(Geodasy) was placed on a two-circle goniometer (OWIS, with DMT 65, 2-Ph-SM 240) rotated in step-mode.

A frequency doubled CW Nd:Yag laser (Intelite GSLN32-20, $\lambda_{\text{SH}} = 532 \text{ nm}$) was applied to illuminate the ATR substrates from their back-side at different angles of incidence. A secondary cylindrical lens arranged before the ATR half-cylinder composed a telescope to compensate the divergence caused by the light propagation through the half-cylinder. The dependence of the intensity of the reflected light on the angle of incidence was detected by a Si photo-diode (Thorlabs DET110). The step motor controlling and the signal collection were performed by home-made electronics directed via LabVIEW6i. The circle-shaped ATR substrates were rotated applying a special holder and index matching liquid (Schott).

2.4. Atomic force microscopy on polymer gratings

Tapping mode atomic force microscopic study (PSIA) was performed to determine the modulation depth of the polymer gratings generated by two-beam interference. We applied TM AFM tips (NT-MDT NSG11) having a spring constant of 5.5 N/m and resonance frequency of 150 kHz.

3. Results and discussion

The following notation is applied to describe the interacting gratings and the plasmon-field:

- Polymer gratings
 - $G_{\text{grating}1,2}$: period of the grating
 - $a(G_{\text{grating}1,2})$: the modulation depth at the period of the grating
 - $K_{\text{grating}1,2} = 2\pi/G_{\text{grating}1,2}$: wave vector of the grating
- Plasmons
 - Λ_{plasmon} : wavelength of the plasmons
 - $K_{\text{plasmon}} = 2\pi/\Lambda_{\text{plasmon}}$: wave vector of the plasmons
 - φ : resonance minimum on the angle-dependent resonance curve
- Rotated-grating geometry
 - \mathcal{B} : angle between the plasmon propagation direction and the grating normal
 - γ : angle between the plasmon propagation direction and grating grooves (Fig. 1b and c).

3.1. Polymer gratings generated by the interference of two “p” polarized beams

The two-beam interference realized in the arrangement presented in Fig. 1a resulted in a fluence distribution having a period half of the applied master grating:

$$F(x) = F_{\text{average}} \left(1 + V \cos \left(\frac{4\pi x}{G_{\text{master grating}}} \right) \right) \quad (1)$$

where V is the visibility of the interference fringes, F_{average} and $F(x)$ are the average and place-dependent fluences, respectively. The period of the dominant grating-like structure developing on the PC surface corresponds to the periodicity of the interference pattern: $G_{\text{grating}1} = 416$ nm (Figs. 2a and 3a) and

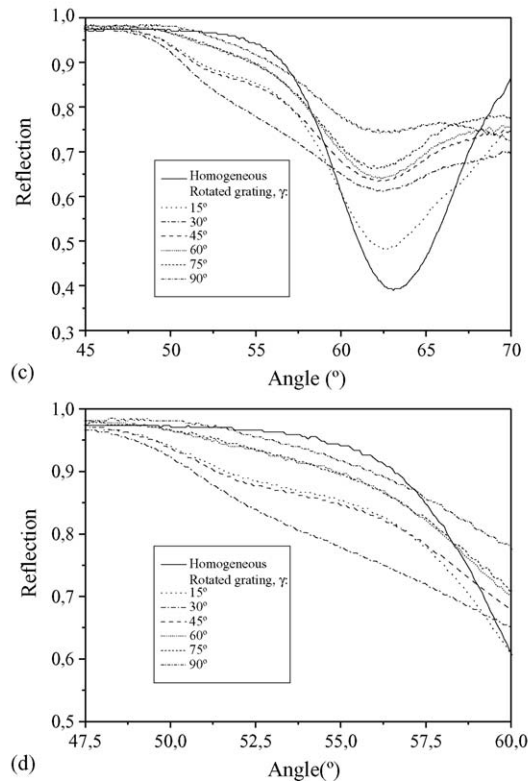
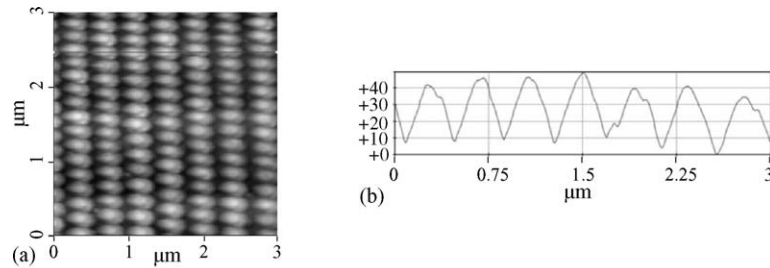


Fig. 2. (a) Polymer grating having a period of $G_{\text{grating}1} = 416$ nm, generated by “p” polarized beam of the fourth harmonic of a Nd:Yag laser: $N = 600$ pulses having a fluence of $F_{\text{av}} = 10.4$ mJ/cm²; (b) line cross-section indicating an average modulation depth of $2a$ (416 nm) = 30 nm; (c) resonance curves measured on rotated gratings, the angle between the grating grooves and plasmon propagation was varied in 15° steps; (d) the grating-coupling is strongest at $\gamma = 30^\circ \approx \gamma_{\text{coupling}}^{n_1=1}$, but it is identifiable also at $\gamma = 15^\circ$ and $\gamma = 45^\circ$ angles.

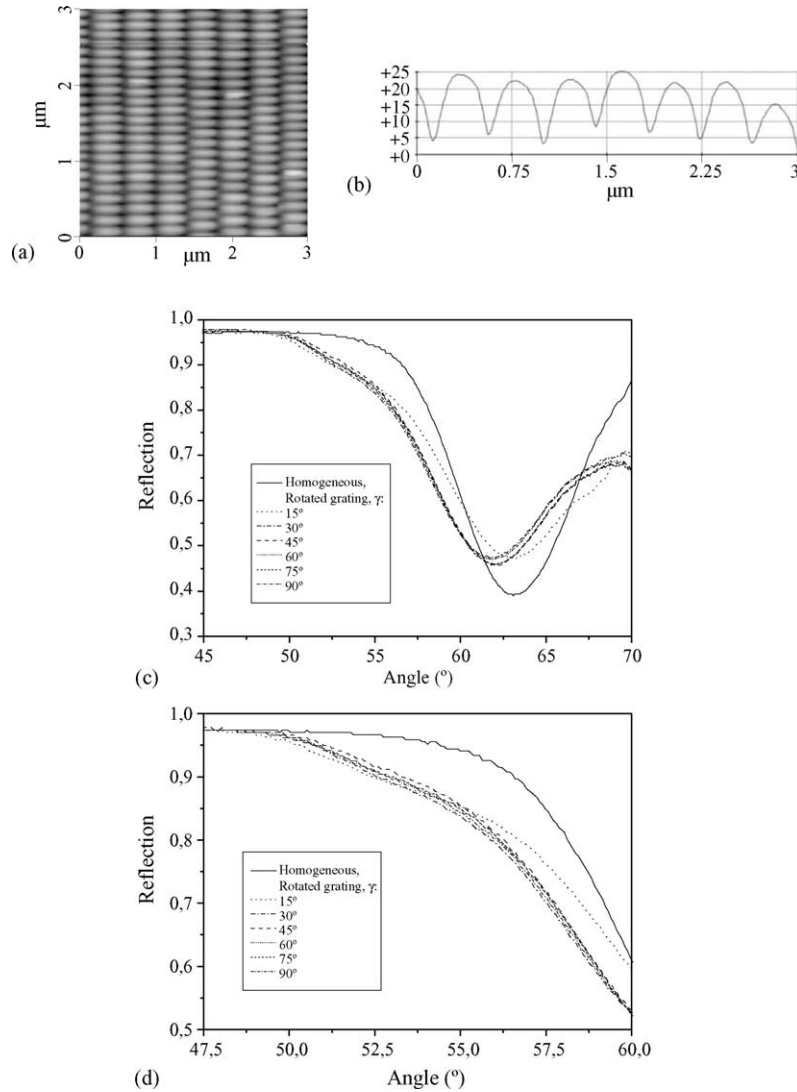


Fig. 3. (a) Polymer grating having a period of $G_{\text{grating}1} = 416$ nm, generated by “p” polarized beam of the fourth harmonic of a Nd:Yag laser: $N = 600$ pulses having a fluence of $F_{\text{av}} = 8.32$ mJ/cm²; (b) line cross-section indicating an average modulation depth of $2a$ (416 nm) = 20 nm; (c) the resonance curves measured on gratings rotated in 15° steps do not show additional resonance peak; (d) the deepest side-wing was detected at $\gamma = 15^\circ$ between the grating grooves and the plasmon propagation.

$G_{\text{grating}2} = 833$ nm (Figs. 4a and 5a) in case of 1200 lines/mm and 600 lines/mm master gratings, respectively. Only in the case of $V = 1$ visibility are the areas corresponding to the intensity minima non-irradiated: $F(x_{\text{min}}) = 0$. In other cases, the fluence is only reduced at the beam-parts corresponding to the minima.

The repeating illumination by “p” polarized beams having a fluence below the ablation threshold results in laser induced periodic surface structure formation [11].

The LIPSS appeared in our case as a secondary droplet-structure arranged parallel to the direction of polarization, i.e. perpendicularly to the grating generated by two-beam interference (Figs. 2–5/a).

The modulation depth of the primary gratings increased as the fluence was increased at the same number of laser pulses. The illumination by $N = 600$ laser pulses having a fluence of $F_{\text{av}} = 10.4$ mJ/cm² resulted in a modulation depth of $2a$ (416 nm) = 30 nm (Fig. 2b), while in case of $F_{\text{av}} = 8.32$ mJ/cm²

a smaller depth of $2a$ (416 nm) = 20 nm was measurable on the line cross-section of the AFM pictures (Fig. 3b). Comparing the AFM pictures taken about PC layers illuminated by laser beams having the same fluence but applying different number of laser pulses we concluded that the increase of the number of shots also resulted in deeper structures. The grating generated by laser beam having a fluence of $F_{\text{av}} = 15.6$ mJ/cm² has a modulation depth of $2a$ (833 nm) = 30 nm after $N = 300$ laser pulses (Fig. 4b), while $N = 100$ pulses caused smaller average modulation depth of $2a$ (833 nm) = 20 nm (Fig. 5b).

3.2. Theoretical considerations about the dependence of the grating-coupling phenomenon on the period, angle of rotation and modulation depth of the polymer gratings

The covering of the silver layer by dielectric film causes the plasmon resonance peak to shift to a larger angle depending on

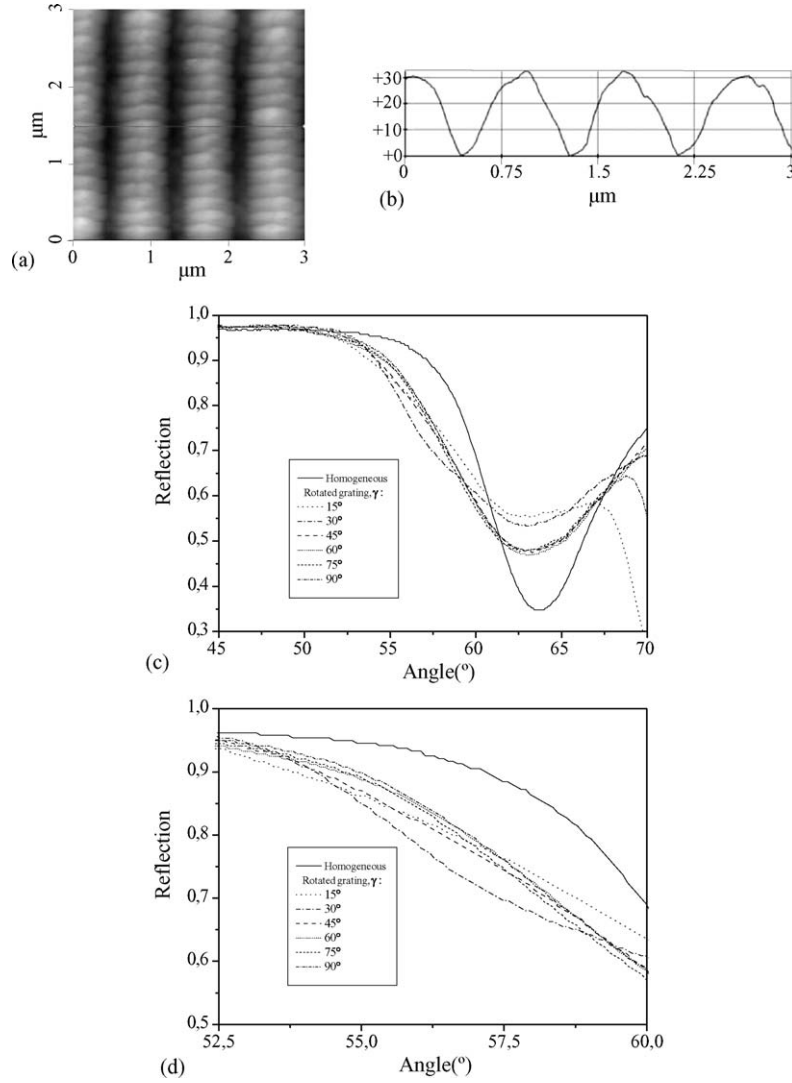


Fig. 4. (a) Polymer grating having a period of $G_{\text{grating}2} = 833$ nm, generated by “p” polarized beam of the fourth harmonic of a Nd:Yag laser: $N = 300$ pulses having a fluence of $F_{\text{av}} = 15.6$ mJ/cm²; (b) line cross-section indicating an average modulation depth of $2a$ (833 nm) = 30 nm; (c) resonance curves measured on rotated gratings, the angle between the grating grooves and plasmon propagation was varied in 15° steps; (d) the grating-coupling is well defined at $\gamma = 30^\circ \approx \gamma_{\text{coupling}}^{n_2=2}$.

the film thickness. The K_{plasmon} wave vector of the surface plasmon propagating at the polymer–silver interface can be determined as follows:

$$K_{\text{plasmon}} = \frac{2\pi}{\Lambda_{\text{plasmon}}} = \frac{2\pi}{\lambda_{\text{SH}}} n_{\text{glass}} \sin \varphi \quad (2)$$

where Λ_{plasmon} plasmon wavelength can be calculated based on the φ resonance position, and n_{glass} (532 nm) = 1.519 is the index of refraction of the NBK7 at the measuring wavelength.

The presence of a periodic roughness may result in a coupling phenomenon, the angle between the plasmon propagation direction and the grating normal, where an optimal coupling effect occurs is:

$$\cos \vartheta_{\text{coupling}}^n = \frac{n K_{\text{grating}}}{2 K_{\text{plasmon}}} \quad (3)$$

where $K_{\text{grating}1,2} = 2\pi/G_{\text{grating}1,2}$ are the grating wave vectors. The $K_{\text{coupled plasmon}}^n$ wave vector of the coupled plasmon can be determined as a projection of the original one (Fig. 1c):

$$K_{\text{coupled plasmon}}^n = K_{\text{plasmon}} \cos \gamma_{\text{coupling}}^n = \frac{2\pi}{\lambda_{\text{SH}}} n_{\text{glass}} \sin \varphi_{\text{coupling}}^n \quad (4)$$

where $\gamma_{\text{coupling}}^n$ is the angle between plasmon propagation direction and the grating grooves, $\varphi_{\text{coupling}}^n$ is the direction, where we expect an additional peak in the resonance curve in case of coupling. Rearranging the relation between the change in the plasmon wave-vector and the modulation amplitude of the grating on the dielectric layer [6]:

$$\begin{aligned} \frac{\delta K_{\text{plasmon}}}{K_{\text{plasmon}}} &= \frac{K_{\text{plasmon}} - K_{\text{coupled plasmon}}^n}{K_{\text{plasmon}}} \\ &= \frac{4 K_{\text{plasmon}}}{\sqrt{\varepsilon_{1,\text{PC}}}} \cdot a_{\text{coupling}}^n \sin^2 \gamma_{\text{coupling}}^n \end{aligned} \quad (5)$$

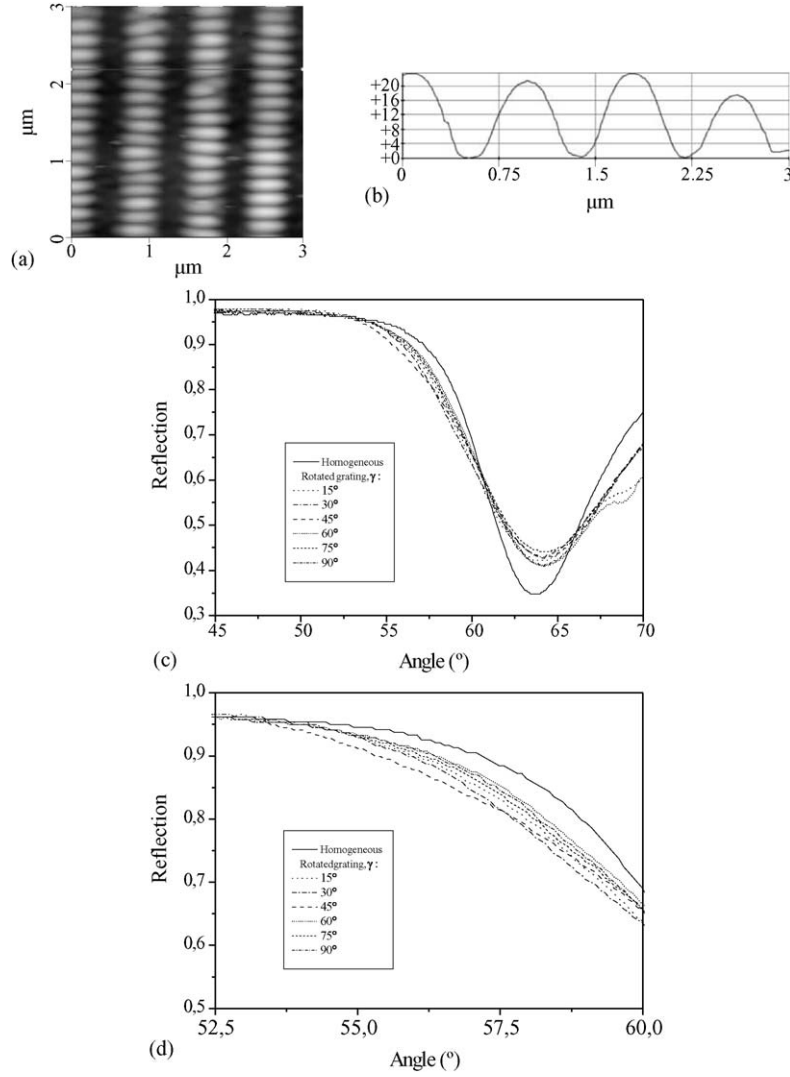


Fig. 5. (a) Polymer grating having a period of $G_{\text{grating}2} = 833$ nm, generated by “p” polarized beam of the fourth harmonic of a Nd:Yag laser: $N = 100$ pulses having a fluence of $F_{\text{av}} = 15.6$ mJ/cm²; (b) line cross-section indicating an average modulation depth of $2a$ (833 nm) = 20 nm; (c) the resonance curves measured on gratings rotated in 15° steps do not show additional resonance peak; (d) the deepest side-wing was detected at $\gamma = 45^\circ$ between the grating grooves and the plasmon propagation.

we can give a condition for the appropriate modulation depth, which is required to exist for the appearance of an additional peak. For different angles of rotation we can calculate:

$$a_{\text{coupling}}^n \sin^2 \gamma_{\text{coupling}}^n = \frac{\sin \varphi - \sin \varphi_{\text{coupling}}^n}{\sin^2 \varphi} \frac{\sqrt{\varepsilon_{1,\text{PC}}}}{4(2\pi/\lambda_{\text{SH}})n_{\text{glass}}} \quad (6)$$

and it is important to emphasize that the original resonance position is implicitly included in the first term of the equation. The consequence, which has to be considered in practical applications, is that at the given propagation direction the modulation depth necessary to result in detectable coupling depends on the original film thickness.

We determined the conditions for the optimal grating-coupling based on the Eqs. (3)–(6) for polymeric surface gratings having periods of $G_{\text{grating}1} = 416$ nm and $G_{\text{grating}2} = 833$ nm

(Table 1). Based on these calculations, we expect detectable coupling in case of $\gamma_{\text{coupling}}^{n_1=1} = 28.2^\circ$ and $\gamma_{\text{coupling}}^{n_2=2} = 28^\circ$ angles between the grating grooves and a plasmon propagation direction. Caused by the commensurability of the wave vectors of the plasmons and that of the grating in case of the smaller periodicity: $K_{\text{plasmon}} = \frac{2\pi}{\Lambda_{\text{plasmon}}} > \approx \frac{2\pi}{G_{\text{grating}1}} = K_{\text{grating}1}$, there is no other favored direction, while in case of the larger periodicity one more direction $\gamma_{\text{coupling}}^{n_2=1} = 13.6^\circ$ may result in the emergence of an additional peak.

3.3. Experimental evidence of the dependence of plasmon coupling phenomenon on the period, angle of rotation and modulation depth of the gratings generated by two-beam interference

The dielectric constants given in the literature resulted in appropriate agreement between the plasmon resonance curves measured and calculated in case of pure metal layers [12]. We

Table 1
The coupling conditions

N	$G_{\text{grating1}} = 416 \text{ nm}, \varphi = 63.1^\circ$				$G_{\text{grating2}} = 833 \text{ nm}, \varphi = 63.7^\circ$			
	$\gamma_{\text{coupling}}^n$ ($^\circ$)	$\vartheta_{\text{coupling}}^n$ ($^\circ$)	$\varphi_{\text{coupling}}^n$ ($^\circ$)	a_{coupling}^n (nm)	$\gamma_{\text{coupling}}^n$ ($^\circ$)	$\vartheta_{\text{coupling}}^n$ ($^\circ$)	$\varphi_{\text{coupling}}^n$ ($^\circ$)	a_{coupling}^n (nm)
1	28.2	61.8	51.8	13.2	13.6	76.4	60.6	12.5
2	19.3	70.7	17.1	–	28	62	52.4	13.1
3	–	–	–	–	44.7	45.3	39.6	–
4	–	–	–	–	69.7	20.3	18.1	–

applied the following dielectric constants to fit the resonance peaks measured on the ATR samples covered by PC film: $\varepsilon_{1,\text{Ag}} = -11.6$, $\varepsilon_{2,\text{Ag}} = 0.38$; $\varepsilon_{1,\text{Al}_2\text{O}_3} = 3.1427$, $\varepsilon_{2,\text{Al}_2\text{O}_3} = 0$; $\varepsilon_{1,\text{PC}} = 2.53$, $\varepsilon_{2,\text{PC}} = 0$. The thickness of the intact PC layer determined based on the ATR measurements on homogeneous areas was: $d_{\text{PC},1} = 46.75 \text{ nm}$ and $d_{\text{PC},2} = 47.5 \text{ nm}$, in case of samples presented in Figs. 2 and 3 and Figs. 4 and 5, respectively. The enhanced broadening of the measured curve compared to calculated resonance peaks was explained by the $\Delta d_{\text{PC}} = \pm 2.5 \text{ nm}$ thickness distribution of the untreated polymer film.

In our experiments, we rotated the ATR substrates in 15° steps, and investigated the angle dependence of the reflection at six different orientations. We observed the emergence of additional peaks arising from grating-coupling effect for both of the periodicities, when the modulation depth was appropriately large of $2a = 30 \text{ nm}$ (Figs. 2c and d and 4c and d).

The strongest coupling resulting in the deepest additional resonance peak was experienced at $\gamma = 30^\circ$, in accordance with the calculated condition of an optimal coupling (Table 1). The additional peaks starts on the resonance curves at the calculated angles $\varphi_{\text{coupling}}^{n_1=1} = 51.8^\circ$ and $\varphi_{\text{coupling}}^{n_2=2} = 52.4^\circ$, but they are not separated from the original resonance peak, on the contrary we found continuous side wings. The coupling effect was still well defined in case of $\gamma = 15^\circ$ and $\gamma = 45^\circ$ angles between the grating groves and plasmon propagation direction on the grating having the smaller periodicity (Fig. 2c and d). A second additional minimum at $\varphi_{\text{coupling}}^{n_2=1} = 60.6^\circ$ was non-detectable caused by its small distance from the original peak in case of PC films comprising a grating having the larger periodicity (Fig. 4c and d). The depth of the side wings decreased, and no real grating-coupling was detectable at larger rotation angles: $\gamma = 60^\circ$, 75° , 90° on neither of the gratings. The deviations from the calculated positions, the broadening and the continuous transition between the peaks can be explained by the complex surface structure. The modulation depth distribution corresponding to Gaussian illuminating beam, the non-rectangular surface profile of the primary grating and the rotation angle dependent scattering of the droplets contribute to these effects.

Similar set of measurements was performed on gratings having smaller modulation depth of $2a = 20 \text{ nm}$ (Figs. 3c and d and 5c and d). We did not observe real additional minima originating from grating-coupling effect on neither of the gratings. Deeper side wings were detected in case of the grating having smaller periodicity (Fig. 3c and d). The depth of the remnant wings was the largest at $\gamma = 15^\circ$ and $\gamma = 45^\circ$ angles in

case of the $G_{\text{grating1}} = 416 \text{ nm}$, and $G_{\text{grating2}} = 833 \text{ nm}$ gratings, respectively (Figs. 3c and d and 5c and d).

The size of the droplets building up the secondary—LIPSS-like structure is commensurable with the half of the plasmon wavelength, in this way their presence may cause also some localization effects.

We plan to realize measurements on polymer gratings built up from continuous polymer stripes to determine the contribution of the droplets caused scattering to the broadening.

3.4. The explanation of the complex structure based on temperature model calculations

The detected small backshift of the resonance peaks corresponds to small decrease in the average film thickness, which reinforces that material redistribution plays important

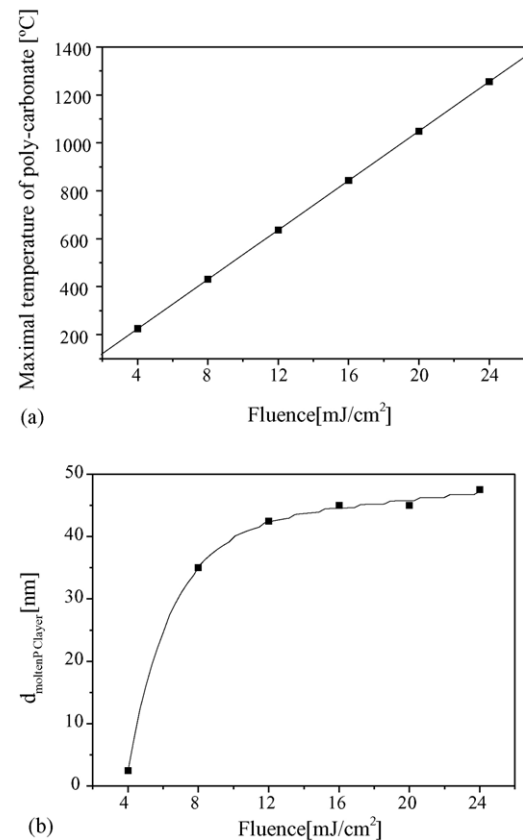


Fig. 6. The maximal temperature in the PC layer as a function of the average fluence for $V = 0.5$ visibility, and $\alpha_{\text{apparent}}(266 \text{ nm}) = 1.9 \times 10^5 \text{ cm}^{-1}$ absorption coefficient.

role in the grating development. We performed temperature model calculations solving the one-dimensional heat flow equation based on the numerical method described in Ref. [13]. The observed droplet formation refers to melting at the hills of the primary grating. Taking into account the probable $V = 0.5$ visibility, an absorption coefficient larger than that of intact PC has to be supposed $\alpha_{\text{apparent}}(266 \text{ nm}) = 1.9 \times 10^5 \text{ cm}^{-1}$ to reach the melting point ($225 \text{ }^\circ\text{C}$) at the interference minima in case of the lowest applied fluence $F_{\text{av}} = 8.32 \text{ mJ/cm}^2$ (Fig. 6). These calculations proved that UV illumination induced incubation plays important role in the structure formation. The chemical changes contribute to material removal causing increased apparent absorption coefficient and resulting in a decrease of the threshold fluences.

4. Conclusions

We generated sub-micrometer polymer gratings consisting of droplets by UV laser-based two-beam interference on the surface of poly-carbonate. The emergence of additional resonance peaks caused by grating-coupling effect was demonstrated in case of two different grating periodicities at rotation angles according to the calculations. It was demonstrated, that the position and depth of the resonance peak is very sensitive to the modulation depth of the grating. This sensitivity reinforces that the grating-coupling phenomenon may be utilized to detect very small amount of materials, which selectively bind into the structure's valley decreasing the modulation depth. The spreading of the additional resonance peak in large angle interval was explained by the scattering effect determined by the complex structure of the grating.

Acknowledgements

Financial support of this research was provided by the SFB Grant no. 1815, and the Hungarian Foundations: OTKA nos. T34825, TS040759 and M41862. M. Csete would like to thank for the János Bolyai Research Scholarship of the Hungarian Academy of Sciences and for the OTKA Hungarian post-doc fellowship D42228. The authors gratefully acknowledge the many discussions with G. Szabó and S. Sarlós. We would like to thank to F. Kárpát for metal layer evaporation and to V. Megyesi for the AFM measurements.

References

- [1] H. Raether, *Surface Plasmons*, Springer, Berlin, 1986.
- [2] S. Puderbach, S. Herminghaus, P. Leiderer, *Phys. Lett. A* 130 (6/7) (1988) 401–404.
- [3] L.A. Moraga, R. Labbé, *Phys. Rev. B* 41 (14) (1990) 10221–10223.
- [4] M. Csete, R. Eberle, M. Pietralla, O. Marti, *Zs. Bor, Appl. Surf. Sci.* 208 (209) (2003) 474–480.
- [5] J. Homola, S.S. Yee, G. Gaultz, *Sens. Actuators B* 54 (1999) 3–15.
- [6] W.L. Barnes, T.W. Persist, S.C. Kitson, J.R. Sambles, *Phys. Rev. B* 54 (9) (1996) 54.
- [7] N. Félidij, J. Aubard, G. Lévi, J.R. Krenn, G. Schider, A. Leitner, F.R. Aussenegg, *Phys. Rev. B* 66 (2002) 1–7.
- [8] C.R. Yonzon, E. Jeoung, S. Zou, G.C. Schatz, M. Mrksich, R.P. Van Duyne, *J. Am. Chem. Soc.* 126 (2004) 12669–12676.
- [9] D.C. Cullen, R.G.W. Brown, C.R. Lowe, *Biosensors* 3 (4) (1987–1988) 211–225.
- [10] H.M. Phillips, D.L. Callahan, R. Sauerbrey, G. Szabó, Z. Bor, *Appl. Phys. Lett.* 58 (24) (1991) 2761–2763.
- [11] M. Csete, *Zs. Bor, Appl. Surf. Sci.* 133 (1998) 5–16.
- [12] Landolt-Börnstein, *New Series III*, 1984.
- [13] A.K. Jain, V.N. Kulkarni, D.K. Sood, *Appl. Phys.* 25 (1981) 127.